Check for updates

# Visualizing screening in noble-metal clusters: static *vs.* dynamic†

Rajarshi Sinha-Roy, [iD] *[abcf] Pablo García-González, [iD] [df] Xóchitl López-Lozano [iD] [e] and Hans-Christian Weissker [iD] *[af]

The localized surface-plasmon resonance of metal nanoparticles and clusters corresponds to a collective charge oscillation of the quasi-free metal electrons. The polarization of the more localized d electrons opposes the overall polarization of the electron cloud and thus screens the surface plasmon. By contrast, a static electric external field is well screened, as even very small noble-metal clusters are highly metallic: the field inside is practically zero except for the effect of the Friedel-oscillation-like modulations which lead to small values of the polarization of the d electrons. In the present article, we present and compare representations of the induced densities (i) connected to the surface-plasmon resonance and (ii) resulting from an external static electric field. The two cases allow for an intuitive understanding of the differences between the dynamic and the static screening.

## Introduction

The response of noble-metal clusters to an external electric field is characterized by the reaction of the metals' electrons. In particular, the well-known effect of the surface plasmon (localized surface-plasmon resonance, LSPR), which dominates the optical absorption spectra of many clusters in the visible and ultraviolet ranges, corresponds to a collective charge oscillation that can be excited by an external field. On the other hand, in the presence of a static external electric field, a static surface polarization is induced that would expel any fields inside the nanoparticle if the latter behaved like a perfect classical metal.[1] Clearly, this leads to differences in the role of the noble metals' d electrons.

It is well known that the basic band structure of the coinage metals/noble metals is rather similar. The delocalized electrons form the metallic sp band, whereas a completely filled shell of

[a] Aix-Marseille University, CNRS, CINAM, Marseille 13288, France.
E-mail: hans-christian.weissker@univ-amu.fr

[b] Laboratoire des Solides Irradiés, École Polytechnique, CNRS, CEA/DRF/IRAMIS, Institut Polytechnique de Paris, Palaiseau F-91128, France

[c] Université de Lyon, Université Claude Bernard Lyon 1, CNRS, Institut Lumière Matière, F-69622, VILLEURBANNE, France.
E-mail: rajarshi.sinha-roy@univ-lyon1.fr

[d] Departamento de Física Teórica de la Materia Condensada and Condensed Matter Physics Center (IFIMAC), Universidad Autónoma de Madrid, E-28049 Madrid, Spain

[e] Department of Physics & Astronomy, The University of Texas at San Antonio, One UTSA circle, 78249-0697 San Antonio, TX, USA

[f] European Theoretical Spectroscopy Facility (ETSF), Web: http://www.etsf.eu

† Electronic supplementary information (ESI) available. See DOI: https://doi.org/10.1039/d2cp04316e

atomic d electrons, which are more localized in space around the atoms, produces the d bands. In the static case, with its approximately vanishing internal fields, the localized d electrons react mostly to the Friedel-oscillation-like density variations of the delocalized electron cloud. They are, therefore, visible in isosurface or color-coded slab representations of the systems, which is why we have likened them to "sensors" in the past.[2]

The d-band edge lies about 4 eV below the Fermi energy in silver and about 2 eV below the Fermi energy in gold and copper. Interband transitions from the d bands, *i.e.*, transitions across the Fermi energy into unoccupied states, start at roughly these energies and are clearly seen in the absorption spectra of the bulk metals.[3] Likewise, the polarizability of the d electrons plays an essential role for the optical response at the nanoscale, in particular leading to the screening of the surface plasmons in the noble-metal clusters.[4–7]

The effect of the noble-metal d electrons on the overall optical response has been taken into account on different levels:

(1) A semiempirical dielectric approximation was implemented into jellium models,[4,6,8–10] where the dynamical polarizability of the d electrons is accounted for by an effective dielectric function $\varepsilon_d(\omega)$. This allowed, in particular, for the description of the size-dependence of the plasmon energies in noble-metal clusters due to the size-dependent influence of different surface effects, *viz.*, the electron spill-out and the reduced screening of the d electrons in a surface layer of the cluster. This approach also served to understand the behavior of the dispersion relation of surface plasmons at noble-metal surfaces.[11–13]

This journal is © the Owner Societies 2023

*Phys. Chem. Chem. Phys.*, 2023, **25**, 2075–2083 | **2075**

(2) In later works,[5,14] d electrons were introduced as point dipoles depending on the surrounding density and introduced in an averaged manner into a jellium model. Nevertheless, as in the dielectric approximation, the response of the d electrons is treated at a different level of theory than that of the valence-electrons.

(3) Newer calculations[7,15–20] describe the electron–core inter-action using suitable pseudopotentials,[21] effective core poten-tials, or PAWs[22] in the framework of Time-Dependent Density-Functional Theory (TDDFT)[23] or sometimes quantum-chemistry methods.[24] As a consequence, the d and the sp electrons are treated explicitly at the same level of theory, whereas the more strongly bound core electrons below are considered as negligi-ble for the optical response and compounded into the pseudopotential.

In present-day calculations of metal clusters, TDDFT has mostly become the method of choice. More generally, plasmonic features in a wide variety of situations have been described by TDDFT, ranging from bulk plasmons in metals[25] and semiconductors[26] to plasmons in molecules[27] and metal clusters.[28] In addition, the correspondence between the classical and the quantum results was analyzed in ref. 29.

In particular, the real-time formalism of TDDFT[30,31] obtains the evolution of the induced densities, which provides an intuitive way of understanding the processes involved in the excitations. As the d electrons are more localized than the metals' sp electrons, it is easy to distinguish the two in representations of the induced densities even without explicit analysis using projections, because small spatial shifts lead to smaller differences for the smooth, extended sp contributions compared to the more strongly peaked d-state densities.[7,16,31]

In earlier work, we have used snapshots and animations[32,33] from $\delta$-kick RT-TDDFT calculations[30] to discuss the electron dynamics. This approach is, however, really useful only if the electron dynamics is dominated by one mode,[33] otherwise, the superposition of different modes complicates the interpreta-tion enormously. We have then, in order to resolve contribu-tions of different frequencies to the absorption spectra, used a Fourier transform analysis of the time-dependent density for each space point, so as to obtain electronic oscillation modes belonging to particular frequencies and representing individual peaks in the spectra.[31]

In the present article, we illustrate and discuss in an intuitive manner the differences in the reaction of the d electrons in the dynamic (plasmonic) case and in the static case, thereby emphasizing their role in the screening in the clusters.

## Methods

As model structures, we use the icosahedral $Ag_{309}$ quasi-spherical silver cluster from the series of icosahedral closed-shell clusters that we have extensively studied before.[2,34] In addition, a silver nanorod of 263 atoms is used. This type of rods based on 5-fold symmetry axes has likewise been studied

extensively before.[29,35–37] These decahedral rods are model structures based on a stacking and shell-wise expansion of decahedral base clusters like the $Au_{13}$. Such decahedral shapes are competitive for some materials and sizes.[38] In addition to the pentagonal rods, rod-like structures cut-out of the fcc bulk material have been used in the discussion of aspect-ratio dependence and general shifts of surface-plasmon energies.[39,40]

The $Ag_{309}$ was relaxed using the VASP code.[41,42] The $Ag_{263}$ rod was not relaxed.

The electronic states and the optical spectra have been calculated using DFT and TDDFT with the real-space code octopus.[43] Norm-conserving Troullier–Martins pseudopotentials[44] were used which include the d electrons in the valence, that is, with 11 valence electrons for each atom. The gradient-corrected PBE exchange–correlation functional[45] has been used. The real-space grid spacing was set to 0.18 Å, the radius of the spheres around each atom that make up the calculation domain was set to 5 Å.

Optical spectra were calculated using the Yabana–Bertsch time-evolution formalism[30] of TDDFT using the real-space code octopus[43] and the gradient-corrected PBE exchange–correlation potential. The ETRS propagator ("enforced time-reversal sym-metry") was used. Propagation time was 25 fs.

In order to analyze the electronic modes contributing to the individual features in the absorption spectra, we used the Fourier-transform analysis of the time-dependent induced density from a $\delta$-kick RT-TDDFT calculation that some of the present authors recently presented and analyzed in detail.[31] The time-dependent induced densities for each 25th time-step were used to perform the Fourier transformation at each of the grid points. The grid spacing (0.18 Å), the interval between two consecutive time-steps ($dt = 0.0024\hbar$ $eV^{-1}$), and the total time of evolution ($12\,500 \times dt$) were chosen to be the same as in the octopus simulation for the corresponding spectra. A damping of 0.0037 atomic units of energy ($\approx 0.1$ eV) was chosen for the exponential window function during the Fourier transform.

The modes of the induced density corresponding to the optical absorption at a given energy $\omega$ are shown as the Fourier sine coefficients which were written out for 100 equally spaced frequency points between 0 and 0.27 atomic units of energy (*i.e.*, up to 7.35 eV). We show the sine coefficients of the Fourier transform because, for a well resolved excitation peak in the absorption spectrum centered at a given energy $\omega$, they corre-spond to the induced densities at $T/4$, $T$ being $2\pi/\omega$.[31]

### Static calculations

Using the real-space code octopus,[43] we calculate both the the field-free ground state and the ground state with a constant and homogeneous external electric field $E = 0.2$ eV $Å^{-1} = 0.00389$ $E_h$/$(ea_B)$, where $E_h$ is the Hartree energy and $a_B$ is the Bohr radius. The field, which is arbitrary but small enough to guarantee a linear response of the electron system, is applied along one of the five-fold symmetry axes in all cases. The same pseudopo-tentials, PBE functional, grid spacing and radius as in the dynamic calculations were used.

**2076** | *Phys. Chem. Chem. Phys.*, 2023, **25**, 2075–2083

This journal is © the Owner Societies 2023

# Results: static vs. dynamic screening

We consider first the icosahedral quasi-spherical 309 atom silver cluster $Ag_{309}$, the spectrum of which is shown in Fig. 1. In the left column of Fig. 2, the dynamic response at the surface plasmon energy is shown, *i.e.*, the induced density obtained by the Fourier-transform tool described in the Methods section. The calculations using the PBE functional have a number of shortcomings. In particular, they underestimate the SPR energies,[46] but the qualitative picture is well represented. A comparison with the long-range-corrected LB94 functional for a smaller silver rod is shown in the ESI.† The expected dipole mode of the collective charge oscillation that characterizes the LSPR in spherical or quasi-spherical clusters is clearly visible, in particular when the induced density of the system is represented using isosurfaces of a rather small density in Fig. 2(a), such that the pictured contributions belong mainly to the delocalized sp electrons. The influence of the different isovalues is discussed below and illustrated in Fig. 4.

This surface mode of the delocalized electrons is connected with the d electrons that oscillate with the same frequency (which is not their resonance frequency) but out of phase with the surface contribution. This polarization, opposing the surface mode, is nothing else but the dynamical screening by the d electrons as mentioned above.[5,6,16,31,33] In particular, around each atom we observe the localized contribution opposed to the surface mode. This is even more clearly seen in the color-coded slab representation of the same system in Fig. 2(b) and (c) where around each of the atoms that sit on the slab, the polarization opposing the field of the outer electron cloud is clearly visible by the change of colors opposite to that of the latter. Finally, the same is seen in the density line profile in Fig. 2(d) where clearly each atom sits approximately at a zero

point within an interval of increasing density, illustrating the same situation.

The situation is very different for the static response, *i.e.*, the induced density due to a static, homogeneous external electric field, shown in Fig. 2(e–h). Even though the overall picture as seen from outside the structure is likewise an overall dipole, the density is very different here. We have studied this situation in detail in order to discuss the metallicity of noble-metal clusters.[2] If the NPs were classical perfect metals, the interior fields would be strictly zero, with surface charges compensating any imposed fields inside. In particular, if a cavity existed in such a structure, it would be invisible to a static electric field. Using the overall static polarizability of the clusters as a measure, we have shown previously that the NPs of about 300 atoms are clearly metallic—as little as one layer of atoms is sufficient to produce about 96% of the polarization of the corresponding compact structure.[2] The static screening is, in fact, very close to that of a classical perfect metal. Nonetheless, the structures exhibit the Friedel-oscillation-like modulations of the density as they are well known to occur at metallic surfaces and in clusters. These density variations, as they occur for simple metals and jellium models alike, are also present in the noble-metal clusters. Clearly, they concern the delocalized electron density of the sp bands. By contrast, the d electrons act somewhat as "sensors" there, in the sense that they react to the local surrounding density and, therefore, make the density variations easily visible in the representations of the induced density. Naturally, unlike in the dynamic case, here the d electrons are not systematically opposing the (surface) dipole polarization of the delocalized electron cloud.[2] Furthermore, as the field inside the cluster is largely screened, *i.e.*, the field inside roughly vanishes, there is little contribution by the d electrons to the static response. This is most clearly seen in the density line profile along the central axis of the cluster shown in Fig. 2(h) which shows rather small variations compared to the dynamic case (as referred to the scale of the induced-density maxima at the surfaces).

The situation is even clearer in the second example that we use here: that of a quasi-1d structure, the nanorod $Ag_{263}$. It has two advantages over the quasi-spherical cluster: (1) the structure is quasi-one-dimensional and the induced densities are, therefore, easier to interpret than the ones above where the shape (facets...) renders the picture more intricate, and (2) the fact that the LSPR is strongly red-shifted compared to the spherical structure.[29,36,37] The optical absorption spectrum is shown in Fig. 1. This separates the excitation further from the interband transitions and makes the interpretation clearer.

The dynamic response at the surface-plasmon frequency (*cf.*, the spectrum in Fig. 1) is shown in the left-hand side of Fig. 3(a–f), alongside the static density induced by a homogeneous static external electric field in Fig. 3(g–l). Again, low-density iso-surfaces of both situations show an overall dipole. To highlight the effect of the d electrons, we show two different slabs, one cutting through the center axis of the rod, the other parallel to this axis but cutting through the plane defined by the three parallel lines of atoms at the rod's surface.
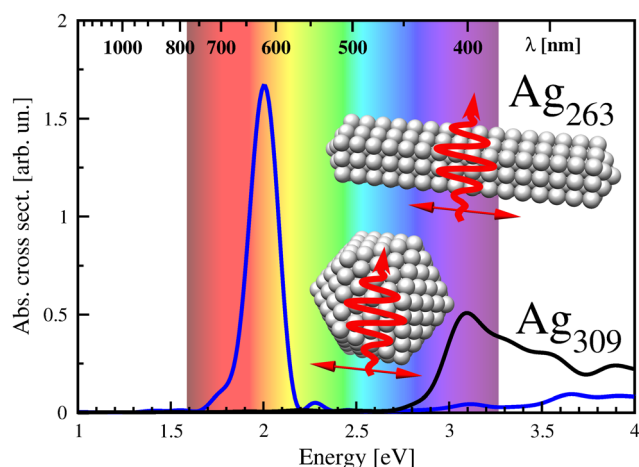


**Fig. 1** Optical absorption spectra of the two systems used for illustration in the present paper, the quasi-spherical icosahedral $Ag_{309}$ and the nanorod $Ag_{263}$. The arrows indicate the direction of the electric field of the optical excitation in the dynamic case, which is identical to the direction of the electric field applied in the static case. The spectrum of $Ag_{309}$ is multiplied by a factor of 5.
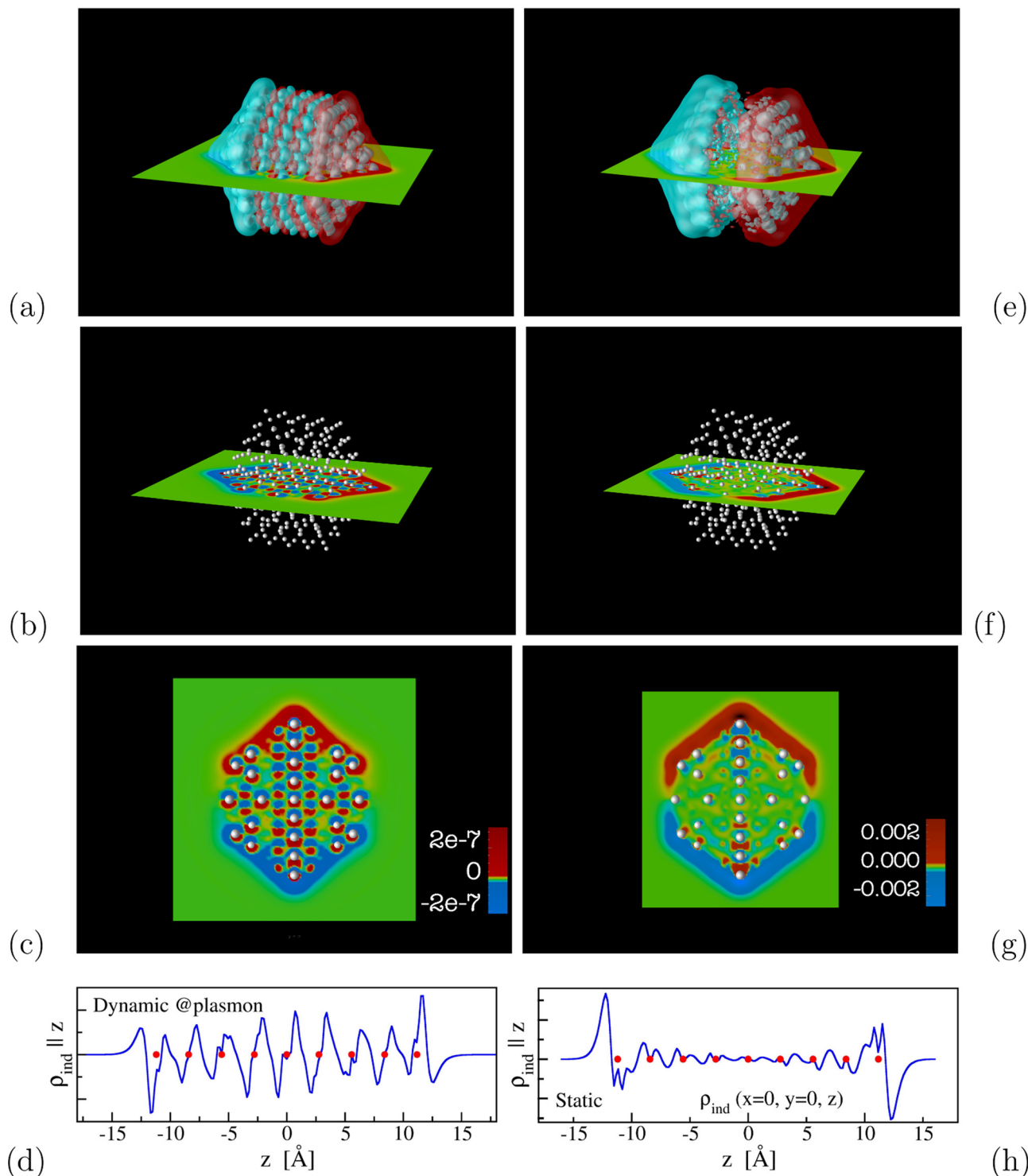
This journal is © the Owner Societies 2023

*Phys. Chem. Chem. Phys.*, 2023, **25**, 2075–2083 | **2077**

Dynamic at plasmon energy          Induced by static electric field



**Fig. 2** Induced densities of $Ag_{309}$ after an optical excitation at the plasmon frequency (left-hand side, a–d) and in response to a static, homogeneous external electric field (right-hand side, e–h). The isosurface representation shows an overall dipole mode of the delocalized electron cloud, the reaction of the d electrons is seen there (the isosurfaces are chosen partly transparent for that reason) and even more clearly in the color-coded slab representations that cut through the center of the cluster. In the slab representations (panels c and g), only those atoms are shown that sit exactly at the center plane or very slightly above and below. These two panels show most clearly the difference of the fields inside the clusters (largely vanishing in the static case) and the reaction of the d electrons (opposing the polarization of the outer electron cloud in the dynamic case, or weakly reacting to the Friedel-oscillation-like modulation of the density in the static case). The lower-most panels show the density along the central axis which is oriented parallel to the excitation, $\rho_{ind}$ $(x = 0, y = 0, z)$.
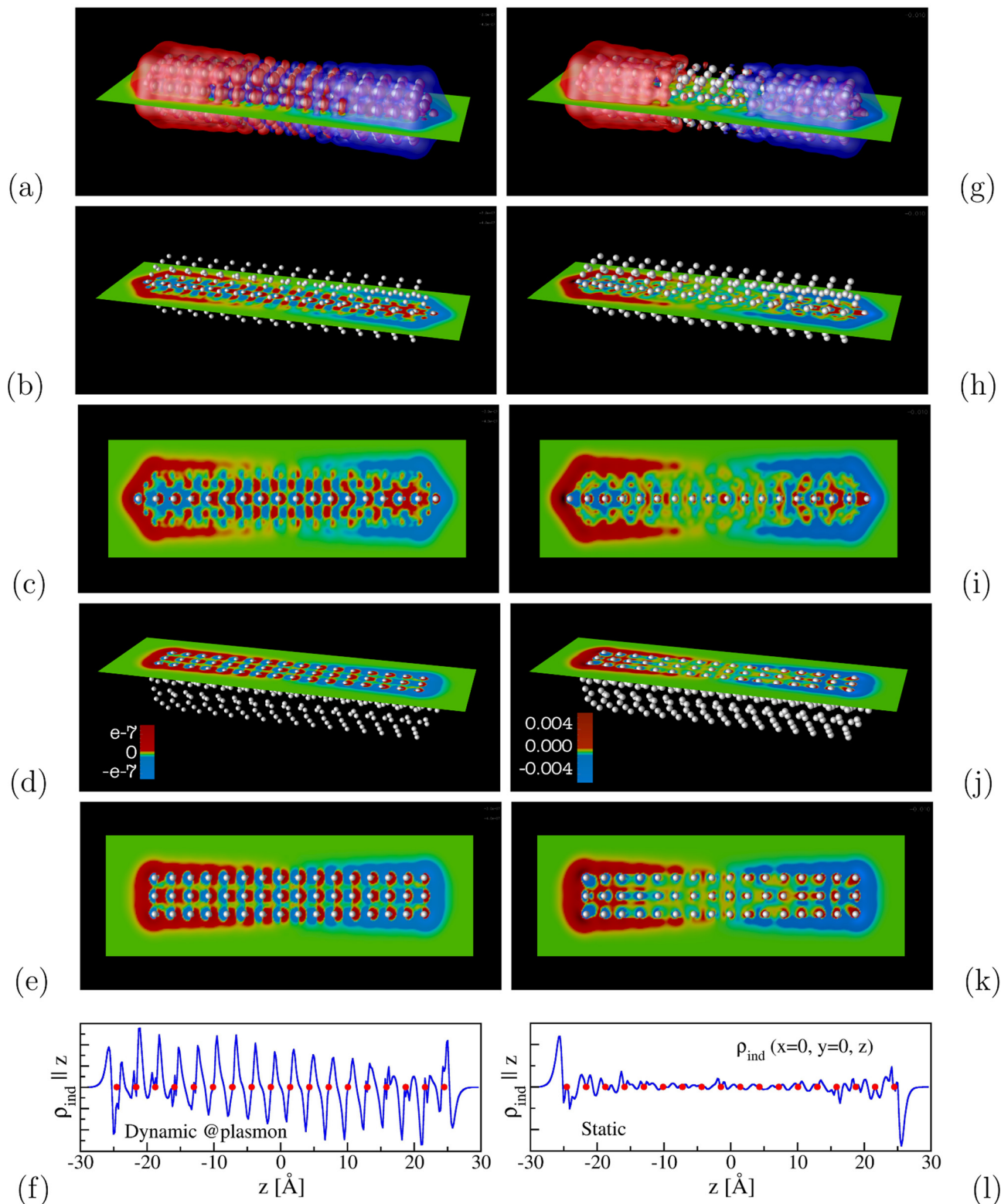
**Fig. 3** Representations of the induced densities of an optical excitation at the SPR frequency and as reaction to a static electric field as in Fig. 2 for the nanorod Ag$_{263}$. The color-coded slab representations of the second and the fourth rows are shown from a perpendicular view angle in the third and the fifths rows for better visibility.

This journal is © the Owner Societies 2023

*Phys. Chem. Chem. Phys.*, 2023, **25**, 2075–2083 | **2079**

**Paper**

View Article Online

**PCCP**

Open Access Article. Published on 10 2565. Downloaded on 29/1/2569 9:19:36. This article is licensed under a Creative Commons Attribution-NonCommercial 3.0 Unported Licence.

Even more clearly than in the quasi-spherical clusters discussed above, we see here that around each of the atoms, the polarization opposes the fields created by the dipole SPR mode. By contrast, in the static case, we see very clearly the strong suppression of the field at the center of the rod, best seen in Fig. 3(i) and (l).

### Intricacies: isovalues and snapshots

The importance of the iso values for how the different contributions can be visualized is illustrated in Fig. 4. There, for the same $Ag_{263}$ nanorod, the iso-surfaces at the plasmon energy are shown for different values of the induced density. Clearly, for the smallest values, the dipole character of the movement of the delocalized electron cloud is visible. An increase of the density values make the contributions of the d electrons clearly visible around each atom. This is a practically important point which has been tacitly used all along this article: the approximate analysis of the interaction of d and sp electrons in noble-metal clusters is possible without an explicit analysis of the wavefunctions' character (projection). But this shows likewise that in the use of iso-surfaces for the visualization of induced densities, care must be taken to make sure that the effects to be discussed are appropriately exposed using appropriate density values.
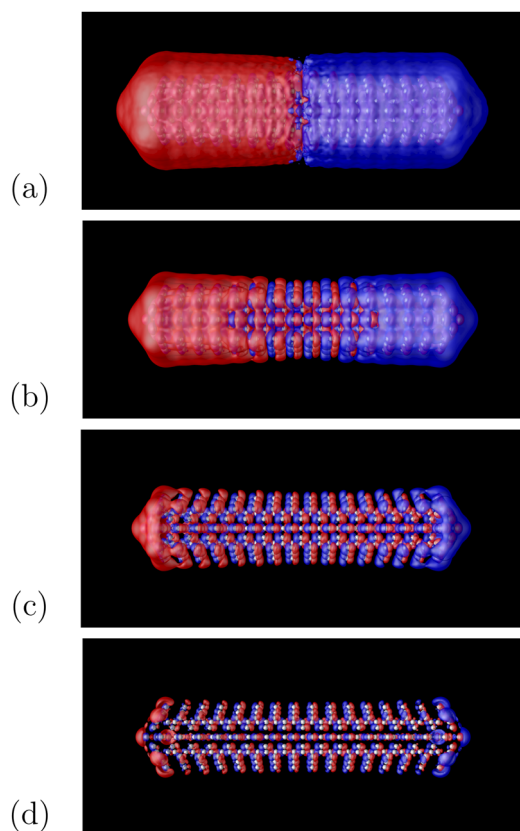
**Fig. 4** Induced density of the $Ag_{263}$ rod after the same optical excitation as shown in Fig. 3, *i.e.*, showing the oscillation at the plasmon frequency. The density of the isosurfaces is progressively increasing, (a) $1 \times 10^{10}$, (b) $1 \times 10^8$, (c) $5 \times 10^8$, and (d) $1 \times 10^7$. The lowest value in (a) highlights the overall dipole mode of the delocalized electrons, whereas with increasing density values, the induced dipoles of the d states around the atoms with opposite polarization become clearly visible.
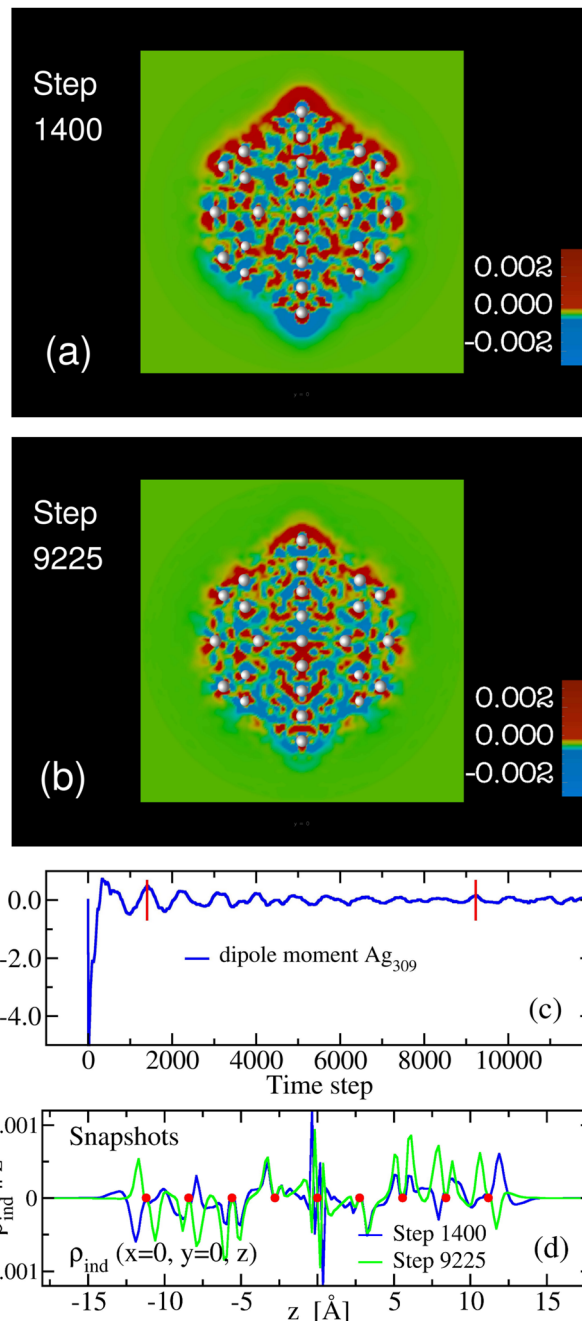
**Fig. 5** (a and b) Slab representations of two snapshots taken out of the trajectory of the $\delta$-kick calculation of $Ag_{309}$. They have been taken at steps 1400 and 9225 of the time evolution, as indicated by the read lines in graph (c) showing the dipole moment as a function of time. The two instants correspond to maximal dipole moments along the evolution. (d) Induced density along the z axis, $\rho_{ind}(x = 0, y = 0, z)$ (*i.e.*, parallel to the excitation direction) for the two snapshots. Clearly, the two snapshots are both much more fuzzy than the Fourier result (Fig. 2(c)). In addition, both the line densities (d) and the slabs show that the densities are very different at the two points in time, even though they have both been taken at instants of maximal overall dipole moment. This shows that the use of snapshots is problematic for situations where more than one mode of any significance are excited, as it is the case for the $Ag_{309}$ at/around the SPR.

In addition, to make the link with previous studies, we comment on the differences of the induced densities obtained

**2080** | *Phys. Chem. Chem. Phys.*, 2023, **25**, 2075–2083

This journal is © the Owner Societies 2023

using the Fourier analysis compared to the snapshots taken out of the trajectories of $\delta$-kick calculations customarily used to calculate optical spectra.

Compared to the snapshots of induced densities from $\delta$-kick calculations (hereafter referred to simply as snapshots) that we have used in the past,[32,33,37] the Fourier analysis allows for much cleaner representations. In the $\delta$-kick calculations, all excitable modes are excited, leading to a superposition of all the respective density oscillations. If there is one dominant mode, with all the rest essentially negligible, one can still draw useful conclusions based on the snapshots out of the trajectories, an example being the rod-like structures that have a very strong resonance for excitation along the long axis which dominates all the response, although even there the pictures are not as "clean" as when the FT analysis is used.[37]

However, looking for instance at spherical clusters (i.e., those most commonly found in experiment), the situation is more intricate. The surface plasmon is fragmented and, in addition, rather close to the onset of the interband transitions from the d electrons. This difference can be seen clearly in Fig. S2 of the ESI,† where we show spectra obtained with a much longer time evolution and the resulting much smaller broadening. While for the rod, a single resonance is dominant compared to all other contributions, in the quasi-spherical $Ag_{147}$, the plasmon is partially fragmented and multiple modes appear close to it. This impacts the snapshots, as we can see clearly in Fig. 5 where two snapshots are compared taken at moments of maximal overall dipole moment. The snapshots are much more fuzzy and thus much more difficult to meaningfully interpret. In addition to the fuzziness, the large differences between the two snapshots taken at different times show that the procedure is rather arbitrary and error prone, in particular if one is tempted to analyze the snapshots in view of an expected result. We note that the multiple modes will influence the Fourier analysis as well if their energetic separation in the spectrum is smaller than the energy window corresponding to the evolution time used, for a detailed discussion we refer to reader to ref. 31.

## Conclusion

In conclusion, we have shown and discussed representations of the induced densities of noble-metal clusters excited at the surface-plasmon frequency and in a static electric field. These representations allow for a direct understanding of, in particular, the role played by the d electrons. In the dynamic case, the screening of the surface mode as seen by the opposite polarization around the atom locations is highlighted. In the static case, where the metallic screening largely suppresses any internal fields, the d electrons react to the Friedel-oscillation-like variations of the density of the delocalized sp electrons. In addition, our illustrations provide a reminder that the density values chosen for isosurface drawings need to be carefully chosen in order to ensure pertinent representations. In particular, a choice of low densities shows very similar overall dipole polarizations for both the dynamic and the static cases,

whereas in reality the two situations are very different due to the metallic screening and the reaction of the d electrons. Moreover, we highlight the need to complement the isosurfaces by slab representations when the interior of the density "clouds" plays a role. Our representations provide an clear picture of the physical situation which, in turn, facilitates the intuitive understanding of the d electron screening.

## Conflicts of interest

There are no conflicts to declare.

## Acknowledgements

## References

1 J. D. Jackson, Classical electrodynamics, Wiley, New York, NY, 2nd edn, 1975.

2 R. Sinha-Roy, P. García-González and H.-Ch. Weissker, How metallic are noble–metal clusters? Static screening and polarizability in quantum-sized silver and gold nanoparticles, Nanoscale, 2020, 12, 4452–4458.

3 P. B. Johnson and R. Christy, Optical Constants of the Noble Metal, Phys. Rev. B: Solid State, 1972, 6, 4370–4379.

4 A. Liebsch, Surface-plasmon dispersion and size dependence of Mie resonance: Silver versus simple metals, Phys. Rev. B: Condens. Matter Mater. Phys., 1993, 48, 11317–11328.

5 L. Serra and A. Rubio, Core Polarization in the Optical Response of Metal Clusters: Generalized Time-Dependent Density-Functional Theory, Phys. Rev. Lett., 1997, 78, 1428–1431.

6 E. Cottancin, G. Celep, J. Lermé, M. Pellarin, J. Huntzinger, J. Vialle and M. Broyer, Optical Properties of Noble Metal Clusters as a Function of the Size: Comparison between Experiments and a Semi-Quantal Theory, Theor. Chem. Acc., 2006, 116, 514.

7 H.-Ch. Weissker, O. Lopez-Acevedo, R. L. Whetten and X. López-Lozano, Optical Spectra of the Special $Au_{144}$ Gold-Cluster Compounds: Sensitivity to Structure and Symmetry, J. Phys. Chem. C, 2015, 119, 11250–11259.

This journal is © the Owner Societies 2023

Phys. Chem. Chem. Phys., 2023, 25, 2075–2083 | 2081

8   J. Tiggesbäumker, L. Köller, K.-H. Meiwes-Broer and A. Liebsch, Blue shift of the Mie plasma frequency in Ag clusters and particles, *Phys. Rev. A*, 1993, **48**, R1749–R1752.

9   G. Toscano, J. Straubel, A. Kwiatkowski, C. Rockstuhl, F. Evers and H. Xu, Asger Mortensen, N.; Wubs, M. Resonance shifts and spill-out effects in self-consistent hydrodynamic nanoplasmonics, *Nat. Commun.*, 2015, **6**, 7132.

10  A. Campos, N. Troc, E. Cottancin, M. Pellarin, H.-Ch. Weissker, J. Lermé, M. Kociak and M. Hillenkamp, Plasmonic quantum size effects in silver nanoparticles are dominated by interfaces and local environments, *Nat. Phys.*, 2019, **15**, 275–280.

11  A. Liebsch, Surface plasmon dispersion of Ag, *Phys. Rev. Lett.*, 1993, **71**, 145–148.

12  J.-S. Kim, L. Chen, L. L. Kesmodel, P. García-González and A. Liebsch, Surface plasmon dispersion of Cl/Ag(111), *Phys. Rev. B: Condens. Matter Mater. Phys.*, 1997, **56**, R4402–R4405.

13  A. Liebsch, Prediction of a Ag multipole surface plasmon, *Phys. Rev. B: Condens. Matter Mater. Phys.*, 1998, **57**, 3803–3806.

14  F. Xuan and C. Guet, Core-polarization-corrected random-phase approximation with exact exchange for dipole surface plasmons in silver clusters, *Phys. Rev. A*, 2016, **94**, 043415.

15  K. Yabana and G. F. Bertsch, Optical response of small silver clusters, *Phys. Rev. A*, 1999, **60**, 3809–3814.

16  M. Kuisma, A. Sakko, T. P. Rossi, A. H. Larsen, J. Enkovaara, L. Lehtovaara and T. T. Rantala, Localized surface plasmon resonance in silver nanoparticles: Atomistic first-principles time-dependent density-functional theory calculations, *Phys. Rev. B: Condens. Matter Mater. Phys.*, 2015, **91**, 115431.

17  R. Schira and F. Rabilloud, Localized Surface Plasmon Resonance in Free Silver Nanoclusters Agn, n = 20-147, *J. Phys. Chem. C*, 2019, **123**, 6205–6212.

18  R. Sinha-Roy, X. López-Lozano, R. L. Whetten and H.-Ch. Weissker, Crucial Role of Conjugation in Monolayer-Protected Metal Clusters with Aromatic Ligands: Insights from the Archetypal Au₁₄₄L₆₀ Cluster Compounds, *J. Phys. Chem. Lett.*, 2021, **12**, 9262–9268, PMID: 34533967.

19  S. Malola, L. Lehtovaara, J. Enkovaara and H. Häkkinen, Birth of the Localized Surface Plasmon Resonance in Monolayer-Protected Gold Nanoclusters, *ACS Nano*, 2013, **7**, 10263–10270.

20  N. A. Sakthivel, M. Stener, L. Sementa, A. Fortunelli, G. Ramakrishna and A. Dass, Au-279(SR)(84): The Smallest Gold Thiolate Nanocrystal That Is Metallic and the Birth of Plasmon, *J. Phys. Chem. Lett.*, 2018, **9**, 1295–1300.

21  E. Luppi, H.-Ch. Weissker, S. Bottaro, F. Sottile, V. Veniard, L. Reining and G. Onida, *Phys. Rev. B: Condens. Matter Mater. Phys.*, 2008, **78**, 245124.

22  P. E. Blöchl, Projector augmented-wave method, *Phys. Rev. B: Condens. Matter Mater. Phys.*, 1994, **50**, 17953.

23  E. Runge and E. Gross, Density-Functional Theory for Time-Dependent Systems, *Phys. Rev. Lett.*, 1984, **52**, 997–1000.

24  V. Bonacic-Koutecky, J. Pittner, M. Boiron and P. Fantucci, An accurate relativistic effective core potential for excited states of Ag atom: An application for studying the absorption spectra of Agn and Agn+ clusters, *J. Chem. Phys.*, 1999, **110**, 3876–3886.

25  S. Huotari, M. Cazzaniga, H.-C. Weissker, T. Pylkkänen, H. Müller, L. Reining, G. Onida and G. Monaco, Dynamical response function in sodium studied by inelastic x-ray scattering spectroscopy, *Phys. Rev. B: Condens. Matter Mater. Phys.*, 2011, **84**, 075108.

26  H.-Ch. Weissker, J. Serrano, S. Huotari, E. Luppi, M. Cazzaniga, F. Bruneval, F. Sottile, G. Monaco, V. Olevano and L. Reining, Dynamic structure factor and dielectric function of silicon for finite momentum transfer: Inelastic x-ray scattering experiments and *ab initio* calculations, *Phys. Rev. B: Condens. Matter Mater. Phys.*, 2010, **81**, 085104.

27  S. Bernadotte, F. Evers and C. R. Jacob, Plasmons in molecules, *J. Phys. Chem. C*, 2013, **117**, 1863–1878.

28  C. Yu, R. Schira, H. Brune, B. von Issendorff, F. Rabilloud and W. Harbich, Optical properties of size selected neutral Ag clusters: electronic shell structures and the surface plasmon resonance, *Nanoscale*, 2018, **10**, 20821–20827.

29  R. Sinha-Roy, P. García-González, H.-Ch. Weissker, F. Rabilloud and A. I. Fernández-Domínguez, Classical and ab Initio Plasmonics Meet at Sub-nanometric Noble Metal Rods, *ACS Photonics*, 2017, **4**, 1484–1493.

30  K. Yabana and G. F. Bertsch, Time-dependent local-density approximation in real time, *Phys. Rev. B: Condens. Matter Mater. Phys.*, 1996, **54**, 4484–4487.

31  R. Sinha-Roy, P. García-González, X. López Lozano, R. L. Whetten and H.-Ch. Weissker, Identifying Electronic Modes by Fourier Transform from δ-Kick Time-Evolution TDDFT Calculations, *J. Chem. Theory Comput.*, 2018, **14**, 6417–6426.

32  H.-Ch. Weissker, R. L. Whetten and X. López-Lozano, Optical response of quantum-sized Ag and Au clusters - cage vs. compact structures and the remarkable insensitivity to compression, *Phys. Chem. Chem. Phys.*, 2014, **16**, 12495–12502.

33  H.-Ch. Weissker and X. López-Lozano, Surface plasmons in quantum-sized noble–metal clusters: TDDFT quantum calculations and the classical picture of charge oscillations, *Phys. Chem. Chem. Phys.*, 2015, **17**, 28379–28386.

34  H.-Ch. Weissker and C. Mottet, Optical properties of pure and core-shell noble–metal nanoclusters from TDDFT: The influence of the atomic structure, *Phys. Rev. B: Condens. Matter Mater. Phys.*, 2011, **84**, 165443.

35  H. E. Johnson and C. M. Aikens, Electronic Structure and TDDFT Optical Absorption Spectra of Silver Nanorods, *J. Phys. Chem. A*, 2009, **113**, 4445–4450, PMID: 19296635.

36  E. B. Guidez and C. M. Aikens, Diameter Dependence of the Excitation Spectra of Silver and Gold Nanorods, *J. Phys. Chem. C*, 2013, **117**, 12325–12336.

37  X. Lopez-Lozano, H. Barron, C. Mottet and H.-Ch. Weissker, Aspect-ratio- and size-dependent emergence of the surface-plasmon resonance in gold nanorods - an ab initio TDDFT study, *Phys. Chem. Chem. Phys.*, 2014, **16**, 1820–1823.

38  F. Baletto, R. Ferrando, A. Fortunelli, F. Montalenti and C. Mottet, Crossover among structural motifs in transition and noble–metal clusters, *J. Chem. Phys.*, 2002, **116**, 3856–3863.

39  G. Piccini, R. W. A. Havenith, R. Broer and M. Stener, Gold Nanowires: A Time-Dependent Density Functional

**2082** | *Phys. Chem. Chem. Phys.*, 2023, **25**, 2075–2083

This journal is © the Owner Societies 2023

Assessment of Plasmonic Behavior, *J. Phys. Chem. C*, 2013, **117**, 17196–17204.

40 R. W. Burgess and V. J. Keast, TDDFT Study of the Optical Absorption Spectra of Bare Gold Clusters, *J. Phys. Chem. C*, 2014, **118**, 3194–3201.

41 G. Kresse and J. Furthmüller, Efficiency of ab-initio total energy calculations for metals and semiconductors using a plane-wave basis set, *Comput. Mat. Sci.*, 1996, **6**, 15.

42 G. Kresse and D. Joubert, From ultrasoft pseudopotentials to the projector augmented-wave method, *Phys. Rev. B: Condens. Matter Mater. Phys.*, 1999, **59**, 1758.

43 N. Tancogne-Dejean, M. J. T. Oliveira, X. Andrade, H. Appel, C. H. Borca, G. Le Breton, F. Buchholz, A. Castro, S. Corni and A. A. Correa, *et al.*, Octopus, a computational framework for exploring light-driven phenomena and quantum dynamics in extended and finite systems, *J. Chem. Phys.*, 2020, **152**, 124119.

44 N. Troullier and J. L. Martins, Efficient pseudopotentials for plane-wave calculations, *Phys. Rev. B: Condens. Matter Mater. Phys.*, 1991, **43**, 1993–2006.

45 J. P. Perdew, K. Burke and M. Ernzerhof, Generalized Gradient Approximation Made Simple, *Phys. Rev. Lett.*, 1996, **77**, 3865–3868.

46 C. M. Aikens, S. Li and G. C. Schatz, From Discrete Electronic States to Plasmons: TDDFT Optical Absorption Properties of Ag n (n = 10, 20, 35, 56, 84, 120) Tetrahedral Clusters, *J. Phys. Chem. C*, 2008, **112**, 11272.

This journal is © the Owner Societies 2023

*Phys. Chem. Chem. Phys.*, 2023, **25**, 2075–2083 | **2083**